

# Plasma Molding Over Surface Topography: Simulation of Ion Flow, and Energy and Angular Distributions Over Steps in RF High-Density Plasmas

Doosik Kim and Demetre J. Economou

**Abstract**—A two-dimensional fluid/Monte Carlo (MC) simulation model was developed to study plasma “molding” over surface topography. The radio frequency (RF) sheath potential evolution, ion density, and flux profiles over the surface were predicted with a self-consistent fluid simulation. The trajectories of ions and energetic neutrals (resulting by ion neutralization on surfaces or charge exchange collisions in the gas phase) were then followed with a MC simulation. In this paper, ion flow, energy and angular distributions of ions, and energetic neutrals bombarding an otherwise planar surface with a step are reported. The step height was comparable to the sheath thickness for the RF high-density plasma considered. As one approaches the step sidewall, the ion flux decreases, the ion energy distribution narrows, and the ion impact angle increases drastically. The ion impact angle at the foot of the step scales with the ratio of sheath thickness to step height. The energetic neutral flux is found to be comparable to the ion flux on the horizontal surface near the step sidewall. Simulation results are in good agreement with experimental data on ion flux and ion energy and angular distributions near the step.

**Index Terms**—Energetic neutrals, Monte Carlo simulation, plasma simulation, sheath over steps, two-dimensional sheath.

## I. INTRODUCTION

LOW-GAS pressure high-charge density plasmas are used extensively for processing of electronic materials, especially for etching and deposition of thin films, as well as surface modification [1], [2]. Examples of high-density plasmas (HDPs) include inductively coupled, helicon, and electron cyclotron resonance discharges. The success of plasma processes depends critically on the flux, energy, and angular distributions of energetic ions bombarding the substrate. In HDPs, the substrate is often biased with an independent radio frequency (RF) power supply to control the energy of ions impacting the substrate. Depending on the ratio of the RF time scale to the ion transit time through the sheath, a broad ion energy distribution (IED) may result [3], [4], [37]. Surface reactions would hardly be affected by low energy ions, while high energy ions could cause damage to the substrate. Also, for anisotropic etch applications with shallow etch-stop layers, ions must arrive perpendicular and uniformly to the substrate. Therefore, controlling

Manuscript received March 14, 2002; revised July 18, 2002. This work was supported in part by Sandia National Laboratories, by the National Science Foundation under Grant CTS-0072854, and by the UH MRSEC Program of the National Science Foundation under Grant DMR-9632667.

The authors are with the Plasma Processing Laboratory, Department of Chemical Engineering, University of Houston, Houston, TX 77204-4004 USA (e-mail: economou@uh.edu).

Digital Object Identifier 10.1109/TPS.2002.805326

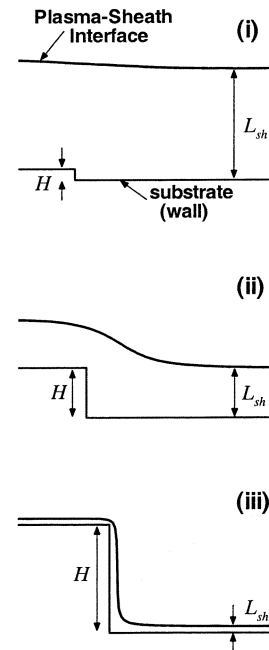


Fig. 1. Plasma molding over a step of height  $H$ . When the sheath thickness  $L_{sh}$  is much larger than  $H$  [ $L_{sh} \gg H$ , case (i)], the plasma-sheath interface (meniscus) is barely perturbed. At the other extreme [ $L_{sh} \ll H$ , case (iii)], the plasma-sheath interface conforms almost exactly to the surface topography. The intermediate case is shown as  $L_{sh} \sim H$  [case (ii)].

the ion flux, IED, and ion angular distribution (IAD) on the substrate are central goals in plasma processing.

Various analytical or numerical models [4]–[8], [37]–[39], as well as experimental measurements [9]–[12] of IEDs and IADs have been reported. In these studies, any surface features on the substrate were extremely small compared to the sheath thickness, i.e., the substrate was effectively planar. There are several applications, however, for which the size of features on the substrate can be comparable to or larger than the sheath thickness. These include plasma source ion implantation, neutral beam processing, plasma thrusters, and the fabrication of microelectromechanical systems [13]–[16]. The plasma would then try to “mold” over the surface topography, i.e., the plasma-sheath boundary or meniscus would not be planar any more. The resulting curved electric field lines can alter the oncoming ion trajectories, greatly influencing the IADs. The ion flux and IEDs along the surface contour would also be affected. Fig. 1 provides a schematic of plasma molding over a step of height  $H$  as an example. In case (i) the sheath thickness,  $L_{sh}$ , is much larger than the step

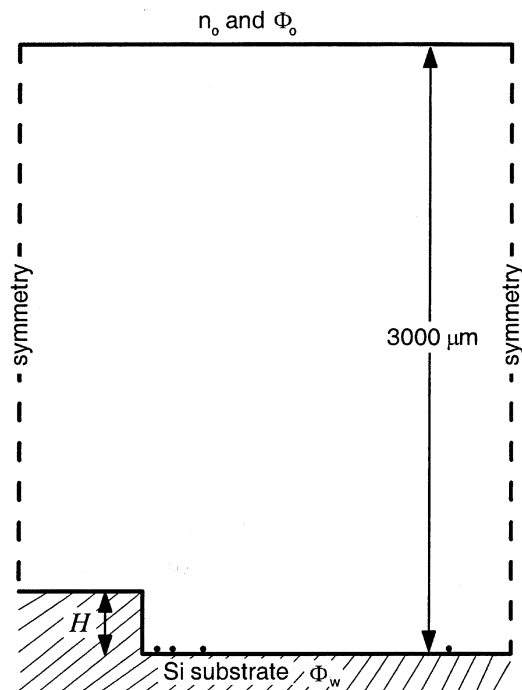


Fig. 2. Computational domain and boundary conditions used for simulations. The electron (ion) density is specified on the upper boundary. The potential is specified on the upper boundary and the Si substrate (wall). Symmetry condition is used on both sides. Small black dots on the substrate to the right of the step represent the four locations (75, 150, 300, and 1500  $\mu\text{m}$  away from the step), where MC kinetic data were collected.

height. The plasma–sheath interface (meniscus) is essentially planar as if the step were nonexistent. In the other extreme [case (iii)],  $L_{sh} \ll H$ , the plasma sheath conforms to the shape of the surface topography. In the intermediate case (ii)  $L_{sh} \sim H$ , the plasma–sheath meniscus “bends” gently over the step. Cases (i)–(iii) would result in drastically different angular distributions of ions impacting the substrate. The flux and IEDs would also be affected. The sheath thickness  $L_{sh}$  depends on the size of the local (evaluated at the sheath edge) Debye length and the sheath potential.

In this article, a two-dimensional (2-D) fluid/Monte Carlo (MC) simulation is reported, in an effort to predict the ion flux, IEDs, and IADs on a surface with a step, in contact with a high-density Ar plasma. Energetic (fast) neutrals resulting by neutralization of ions on the wall or by charge exchange (CX) collisions in the gas were also studied. A description of the model and numerical procedures are presented in Section II. Simulation results and comparison with experimental measurements are discussed in Section III. Conclusions are drawn in Section IV.

## II. SIMULATION

A schematic of the 2-D ( $x, y$ ) system studied is shown in Fig. 2. Away from the step, the sheath is one-dimensional (1-D) and the voluminous literature on 1-D sheaths can be applied. The goal is to study the ion flux, IEDs, and IADs as a function of position along the 2-D step. For this purpose, a combined fluid/MC simulation was employed. The fluid simulation provided the 2-D RF electric field profiles. These were used as input to the MC simulation to follow ion (and fast neutral) trajectories through the sheath and onto the wall.

TABLE I  
PARAMETER VALUES USED FOR SIMULATION

Electron temperature	3.7 eV
Ion temperature*	0.1 eV
Transverse ion temperature*	0.1 eV
Gas temperature	0.05 eV
Gas pressure	5 mTorr
RF frequency	13.56 MHz

\*Used for Monte Carlo simulations only.

### A. Fluid Simulation

An electropositive plasma with one type of positive ions and electrons was considered. The governing equations are the 2-D compressible fluid equations (species and momentum balance) for ions, coupled with Poisson’s equation for the electric potential [2], [17], [18], [40], [19]. The Boltzmann relation was used for the electron density, assuming that the pressure force is balanced by the local electric field force (neglecting electron inertia) [2]. It was further assumed that the ion distribution function is a local drifting Maxwellian. Isothermal equations of state were used for both electrons and ions. The background neutral gas pressure and temperature (hence density) were taken to be constant throughout.

The ion mass and momentum balance equations read

$$\frac{\partial n_i}{\partial t} + \nabla \circ (n_i \vec{u}) = 0 \quad (1)$$

$$\frac{\partial}{\partial t} (n_i \vec{u}) + \nabla \circ (n_i \vec{u} \vec{u}) = -\frac{en_i}{m_i} \nabla \Phi - \nu_m n_i \vec{u} \quad (2)$$

where  $n_i$ ,  $m_i$ , and  $\vec{u}$  are the ion density, ion mass, and ion fluid velocity, respectively.  $\Phi$  is the electric potential and  $e$  is the elementary charge. Ions could suffer either elastic or CX collisions with the background gas. Neither of these processes alters the ion density (no source or sink terms in the ion mass balance). However, these collisions affect the ion momentum as shown by the last term in (2), where  $\nu_m$  is the total collision frequency for momentum loss. Since a drifting Maxwellian is isotropic in the frame moving with the ion drift velocity, a viscous stress term was not included in the momentum equation [17]. The ion pressure force was ignored because the ion temperature is much lower than the electron temperature (cold ions). However, ion thermal effects were accounted for in the MC simulations (see next section).

Poisson’s equation with the Boltzmann relation for electrons reads

$$\nabla^2 \Phi = -\frac{e}{\epsilon_o} \left( n_i - n_o \exp\left(\frac{\Phi - \Phi_o}{T_e}\right) \right) \quad (3)$$

where  $\epsilon_o$  is the permittivity of free space,  $T_e$  is the electron temperature, and  $\Phi_o$  and  $n_o$  are the values for electric potential and ion density, respectively, at the upper boundary (see Fig. 2). Parameter values are shown in Table I.

TABLE II

SUMMARY OF SIMULATION CASES STUDIED IN THIS WORK. FOR CASES (a)–(j), THE POTENTIAL ON THE UPPER BOUNDARY OF FIG. 2 IS  $\Phi_o = 33 + 17 \sin \omega_{RF} t$  V. FOR CASE (k)  $\Phi_o = 50 + 17 \sin \omega_{RF} t$  V AND FOR CASE (l)  $\Phi_o = 70 + 17 \sin \omega_{RF} t$  V. THE ELECTRON TEMPERATURE  $T_e$  IS 3.7 eV AND THE POTENTIAL OF THE WALL  $\Phi_w$  IS 0. THE RESULTING SHEATH THICKNESS (ON A FLAT WALL) AND THE RATIO OF SHEATH THICKNESS TO STEP HEIGHT ( $L_{sh}/H$ ) ARE ALSO SHOWN. GAS PRESSURE AND TEMPERATURE ARE 5 mtorr AND 0.05 eV, RESPECTIVELY. RF FREQUENCY IS 13.56 MHz

case	plasma density on	time-average		$L_{sh}/H$
	upper boundary	sheath thickness*	step height	
	$n_o$ ( $10^{17} \text{m}^{-3}$ )	$L_{sh}$ ( $\mu\text{m}$ )	$H$ ( $\mu\text{m}$ )	
(a)	1.3	295	600	0.485
(b)	1.3	291	300	0.97
(c)	0.2	729	300	2.43
(d)	5.0	152	600	0.253
(e)	0.5	469	600	0.782
(f)	0.5	460	300	1.53
(g)	1.3	296	100	2.91
(h)	0.5	461	100	4.61
(i)	0.2	723	100	7.23
(j)	0.1	1015	100	10.15
(k)	1.3	335	300	1.17
(l)	1.3	382	300	1.27

\* The sheath edge is defined as the position where the relative net charge  $(n_i - n_e)/n_i$  is equal to 0.01, with the densities determined by the fluid simulation. The time-average sheath thickness is calculated 1500  $\mu\text{m}$  away from the step sidewall, where the sheath is one-dimensional. The sheath thickness shows small variation (a few percent) for some cases with the same plasma parameters, but with different step height. This is due to differences in mesh size used in the numerical solution.

Fig. 2 also shows the computational domain and boundary conditions employed in this work. A silicon (Si) substrate is located at the bottom of the domain. A 300- $\mu\text{m}$ -tall step is shown in Fig. 2, although steps with different height (100 and 600  $\mu\text{m}$ ) were also used (see Table II). The electric potential was specified at the top boundary ( $\Phi_o$ ) and on the Si substrate ( $\Phi_w$ ). The Si dopant density was assumed high enough for the substrate to be equipotential (no charging). A symmetry condition ( $\nabla_n \Phi = 0$ ) was applied at the side boundaries. The domain height (3000  $\mu\text{m}$  in Fig. 2), was always much thicker than the sheath thickness (Table II). Hence, the quasi-neutrality condition ( $n_i = n_e = n_o$ ) was applied at the top boundary. The RF plasma sheath evolved self consistently in accordance with the specified plasma parameters ( $n_o$  and  $T_e$ ; effectively, the local Debye length) at the top boundary, and the sheath potential.

At the top boundary, the ion density was specified, but the ion flux was not known. When an ion flux (ion velocity) was also specified, spurious profiles of ion density and flux were observed near the upper boundary. To resolve this issue, the inlet ion vertical velocity  $v_o$  was linearly extrapolated based on the

values at the first two interior nodes  $v_o = 2v_1 - v_2$ . This upstream condition has been used before in compressible gas dynamics simulations [20]. It allows the inlet flux to develop as part of the solution. Simulations started with a specified inlet velocity (for instance,  $v_o = 0.5u_B$ , where  $u_B$  is the Bohm velocity), which was subsequently updated (using the above equation) after each time step. For given plasma parameters, the steady state inlet flux converged to the same value, regardless of the initial value of the inlet velocity.

The governing equations were discretized in space using a finite difference scheme. Conventional higher order ( $\geq 2$ ) schemes are known to suffer from numerical instability and oscillations near steep gradients in highly convective flows, which eventually destroy the solution [20]. To overcome these problems, researchers often use low-order schemes (order 1), such as the upwind or donor cell methods, to discretize the convective terms. Low-order schemes can stabilize the solution, but suffer from excessive numerical diffusion which degrades accuracy. Boris and Book [21] developed the flux-corrected transport (FCT) scheme, in an effort to preserve the advantages

of the low-order and high-order schemes, while at the same time minimizing their disadvantages. In FCT, a weighted-average value of low-order and high-order fluxes is used for the convective terms. The high-order flux is weighted to the maximum extent that allows no instability to be introduced. In this manner, the FCT solutions are stable and also have higher accuracy than low-order solutions. The original FCT scheme was improved and extended to cover multidimensional flows by Zalesak [22]. This algorithm has been used for plasma simulations before [23], [24]. Zalesak's multidimensional algorithm was also used in this work. The time step was chosen so that the Courant–Friedrichs–Levy condition was satisfied. In this study, the Courant number was set to be less than 0.5 [20]. The time step was also set less than 1/200 of the RF cycle time (74 ns). It was assumed that the electric field remained unchanged during a time step. At the end of each time step, Poisson's equation (3) was solved iteratively by a Newton–Raphson method to update the electric potential. The Newton–Raphson algorithm was combined with the conjugate gradient scheme to ensure global convergence. The successive over-relaxation method with Chebychev acceleration was used to invert the Jacobian matrix [25]. Marching in time was continued until a periodic steady state was reached. This normally required 100s of RF cycles.

### B. MC Simulation

If ion flow is collisionless, the ion energy and angular distribution functions at the substrate can, in principle, be calculated knowing the electric field profiles and the initial ion distributions. When ions suffer collisions, however, MC simulation is necessary to calculate the ion distributions at the substrate. The MC simulation procedure used in this work is summarized in Fig. 3. For the flight between collisions (free flight) the equations of motion were integrated using a fourth-order Runge–Kutta method

$$\begin{aligned} \frac{\partial v_x}{\partial t} &= \frac{e}{m_i} E_x(x, y, t) \\ \frac{\partial v_y}{\partial t} &= \frac{e}{m_i} E_y(x, y, t) \\ \frac{\partial v_z}{\partial t} &= 0 \end{aligned} \quad (4)$$

where  $E_x$  and  $E_y$  are electric fields determined by the 2-D fluid simulation, and  $v_x$ ,  $v_y$  and  $v_z$  are components of the particle (not fluid) velocity. The electric field is spatially nonuniform and time varying in the RF cycle. When integrating (4), an ion was not allowed to pass through a mesh cell in a single time step.

Ions with the appropriate energy and angular distributions (see below) were launched near the sheath edge. The launching location was a horizontal plane on which the ion fluid velocity was about  $0.9u_B$ . The location of the ion launching plane was in the transition region between the presheath and the sheath. (At the sheath edge, the ion velocity should be greater than or equal to the Bohm velocity.) Ions were evenly distributed along the launching plane as well as in RF phase (0 to  $2\pi$ ). The position of the launching plane did not influence the results significantly, provided that the launching plane was far enough from

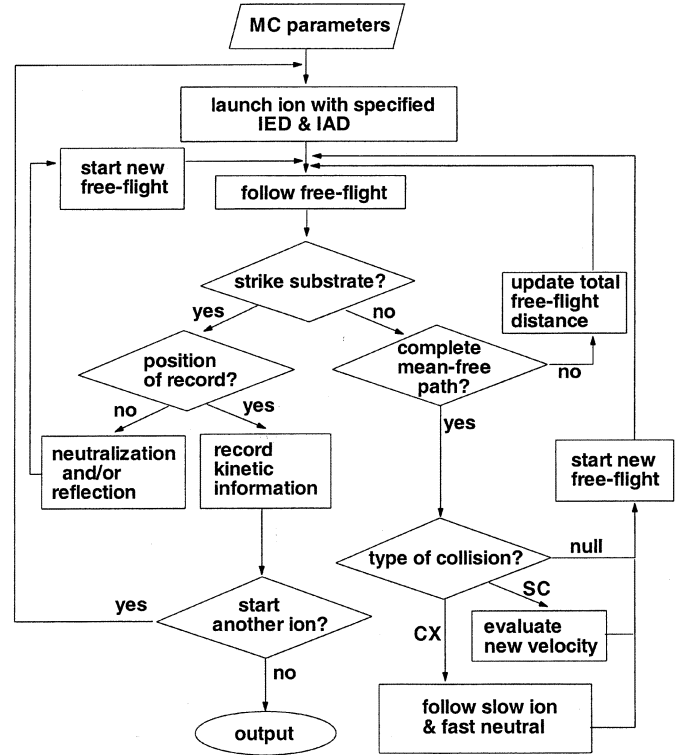


Fig. 3. Flow chart of MC simulation which follows ions and fast neutrals. IED and IAD functions are specified at the input. The simulation accounts for both CX and elastic scattering (SC) collisions in the gas phase. Ion reflection on the sidewall is also accounted for.

the sheath edge. Due to collisions with the background gas in the presheath, ions at the launching plane should have an energy distribution with a spread of order  $T_e$  [26]. The entering ion kinetic energy was determined as follows. The mean energy ( $\epsilon_{\text{mean}}$ ) of ions was first evaluated

$$\epsilon_{\text{mean}} = \frac{1}{2} m_i (u^2 + v^2) \quad (5)$$

using the ion fluid velocities at the launching plane. The ion velocity at this plane was nearly normal, i.e.,  $u \cong 0$ . The ion drift energy ( $\epsilon_{\text{drift}}$ ) was then determined as

$$\epsilon_{\text{drift}} = \epsilon_{\text{mean}} \zeta \quad (6)$$

where  $\zeta$  was picked from a Gaussian distribution

$$f_\zeta(\zeta) = A_\zeta \exp\left(-\frac{1}{2} \left(\frac{\zeta - \mu}{\sigma_\zeta}\right)^2\right) \quad (7)$$

with  $\mu = 1.0$  and  $\sigma_\zeta = 0.4247$  (i.e., the full-width at half-maximum is 1.0). The distribution in (7) was cutoff for  $\zeta \leq 0$  or  $\zeta \geq 2$ . Using (6) and (7), one can generate ion distribution functions at the sheath edge similar to those proposed by Riemann [26]. Collisions in the presheath also cause angular spread of the incoming ions. For the IAD, we used [12]

$$f_\theta(\theta) = A_\theta \exp\left(-\frac{1}{2} \left(\frac{\sin \theta}{\sigma_\theta}\right)^2\right) \quad (8)$$

with

$$\sigma_{\theta} = \sqrt{\frac{T_i, T_r}{2\varepsilon_{\text{drift}}}} \quad (9)$$

where  $T_i, T_r$  is the transverse ion temperature. When compared to that of [12], the angular distribution of (8) is missing a  $\cos^4 \theta$  factor (multiplier), because it was difficult to sample from the distribution function containing this factor. This does not introduce much error. Under conditions of interest here, the IAD at the sheath edge has a spread of only several degrees off normal. For a spread of  $5^\circ$ , for example,  $\cos^4(5) = 0.985$  not far from unity.

The energy and angular distributions of entering ions in (7) and (8) were intended for a 1-D sheath over a planar surface. In order to utilize these distribution functions, it is necessary to launch ions at a position where the influence of plasma molding is negligible. The launching position defined above satisfies this requirement.

During their transit through the sheath, ions can experience SC or charge-exchange (CX) collisions with the background gas (for a pressure of 5 mtorr, however, the sheath is nearly collisionless). The null collision method was employed [27], with a constant total cross section, to evaluate the free flight distance between collision events. At the end of each free flight, the type of collision was determined according to the probability for each collision event: (SC), (CX), and null collision (NU)

$$P_k = \sigma_k / \sigma_{\text{tot}} \\ = \sigma_k / (\sigma_{SC} + \sigma_{CX} + \sigma_{NU}) \quad k = SC, CX, NU. \quad (10)$$

Cross-section data for SC and CX collisions between  $\text{Ar}^+$  and Ar were obtained from [2], and are shown as analytic fits below

$$\sigma_{SC} = 40.04(1.0 - 0.0563 \ln \varepsilon)^2 \quad (11)$$

$$\sigma_{CX} = 47.05(1.0 - 0.0557 \ln \varepsilon)^2 \quad (12)$$

where cross sections are in  $10^{-16} \text{ cm}^2$  and the ion kinetic energy,  $\varepsilon$  is in eV. Due to the mathematical singularity of the logarithmic function, (11) and (12) were cutoff at  $\varepsilon \leq 0.1 \text{ eV}$ . Since the background gas density was assumed to be uniform, the collision probability was determined by the ion kinetic energy at the time of the collision event. SC was treated as a hard sphere collision. For CX collisions, the fast ion and slow neutral switched identity (i.e., became fast neutral and slow ion, respectively) without changing their precollision velocity vector (resonant process). Both the fast neutral and slow ion were followed after the collision. Energetic neutrals could suffer SC further on. Through a series of SCs or reflections on the solid surface, fast neutrals may exit the top boundary (this can not happen for ions). Neutrals exiting the top boundary returned to the bulk plasma and were thermalized. They were not followed any further.

Energetic particle (ions or fast neutrals) scattering on the Si surface is quite complicated [28]. Incidence angle, energy, and surface condition (roughness, contamination) all play a role. Several experimental and/or computational studies [29]–[32] have been reported on the impact of energetic ( $1 \text{ eV} < \varepsilon_i < 1 \text{ keV}$ ) ions on surfaces. The energy and angular distributions of reflected species are still the subject of investigations. The

employed model for surface scattering is the simplest possible and consistent with current knowledge. When impacting, ions lose most of their energy through a series of collisions with surface atoms which may cause ions to be trapped in the surface. Trapped ions were not followed any further in the simulation. The probability for surface trapping was treated as a linear function of incidence angle without energy dependency. Helmer and Graves [31] reported molecular dynamics simulations of  $\text{Ar}^+$  impacts onto bare silicon, showing that the reflection probability increased almost linearly with the impact angle  $\theta_i$  becoming unity for  $\theta_i \geq 80^\circ$ . Following the trend in their data for 50 eV  $\text{Ar}^+$ , the reflection probability ( $R$ ) was assumed to be

$$R = 0.6\theta_i/80 + 0.4 \quad \text{for } \theta_i < 80^\circ \\ = 1 \quad \text{for } \theta_i \geq 80^\circ. \quad (13)$$

In case of reflection, the degree of ion neutralization was assumed to be 100% [32]. It was then assumed that the resulting neutrals reflect specularly (i.e.,  $\theta_i = \theta_r$ ). To calculate the energy transfer, a binary collision model with two half-scatterings was employed [31]

$$\sqrt{\frac{\varepsilon_r}{\varepsilon_i}}(\chi) = \left(\frac{\mu}{\mu+1}\right)^2 \left(\cos \chi_{1/2} + \sqrt{\frac{1}{\mu^2} - \sin^2 \chi_{1/2}}\right)^2 \quad (14)$$

where  $\varepsilon_r$  and  $\varepsilon_i$  are the kinetic energy of reflected and incident particle, respectively. The mass ratio  $\mu \equiv m_{\text{Ar}}/m_{\text{Si}} = 1.4$  in this case. This model assumes that the incident particle experiences two consecutive binary collisions with surface atoms, before being released from the surface. The scattering angle was assumed to be the same for both collisions. The half-scattering angle  $\chi_{1/2}$  is

$$\chi_{1/2} = \frac{\chi}{2} = \frac{\pi - \theta_i - \theta_r}{2} = \frac{\pi}{2} - \theta_i. \quad (15)$$

Helmer and Graves observed that the average energy of reflected Ar from silicon surfaces can be reasonably estimated by the binary collision model.

Kinetic data of ions and fast neutrals were collected and recorded at the substrate to the right of the sidewall of the step. Four locations on the substrate were chosen to facilitate a comparison with experiments: 75, 150, 300, and 1500  $\mu\text{m}$  from the step (see Fig. 2). Table I also shows the base parameter values used for MC simulations.

### III. RESULTS AND DISCUSSION

A summary of the different cases simulated is shown in Table II. In all cases, the base case conditions in Table I were used. The main parameters varied were the step height  $H$ , and the plasma density at the upper boundary (Fig. 2) of the computational domain  $n_0$ . The RF potential of the upper boundary  $\Phi_0$  was also varied. The wall was always at a potential of zero (grounded). The time-averaged sheath thickness over a planar surface  $L_{sh}$  is also shown in Table II. The sheath thickness scales approximately with  $n_0^{-1/2}$  (i.e., Debye length) and shows a rather weak dependency on the potential of the

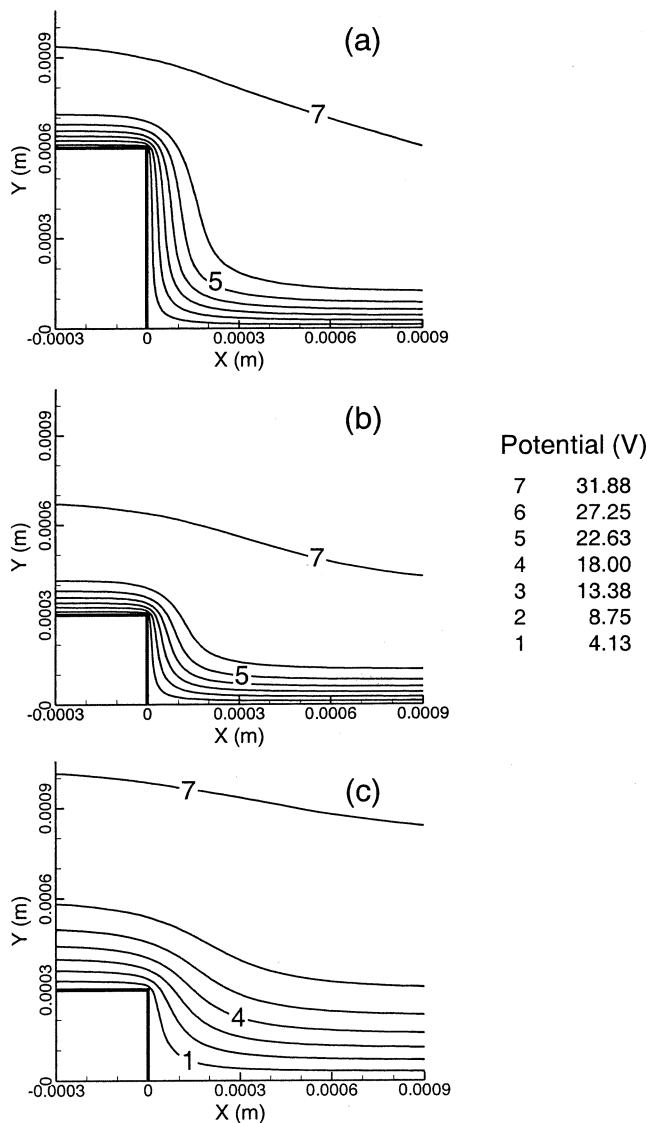


Fig. 4. Contour plots of electric potential at  $\tau_{RF}(\equiv t/2\pi/\omega_{RF}) = 0$ . Cases (a)–(c) correspond to (a)–(c) of Table II: (a)  $n_0 = 1.3 \times 10^{17} m^{-3}$ ,  $H = 600 \mu m$ , and  $L_{sh}/H = 0.485$ , (b)  $n_0 = 1.3 \times 10^{17} m^{-3}$ ,  $H = 300 \mu m$ , and  $L_{sh}/H = 0.97$ , and (c)  $n_0 = 2 \times 10^{16} m^{-3}$ ,  $H = 300 \mu m$ , and  $L_{sh}/H = 2.43$ .

upper boundary (sheath potential in this case). Plasma molding depends on the sheath thickness relative to the step height  $H$ . The simulated range of the  $L_{sh}/H$  ratio was from 0.253 up to 10.2.

Fig. 4(a)–(c) displays electric potential profiles around steps for cases (a)–(c) of Table II, respectively. The sheath thickness is comparable to the step height in all three cases. As a consequence, the plasma “feels” the change of the surface topology, and the sheath “wraps” around the step. The sheath is locally thicker over the step and becomes gradually thinner and planar away from the step. For higher plasma density (i.e., thinner sheath) and/or taller step, the sheath becomes more conformal to the surface topography [compare cases (b) and (c)].

The corresponding electric field vector profiles are shown in Fig. 5. The electric field is very weak outside the sheath and picks up in strength as one enters the sheath near the wall. The electric field vectors are nearly vertical away from the step, but

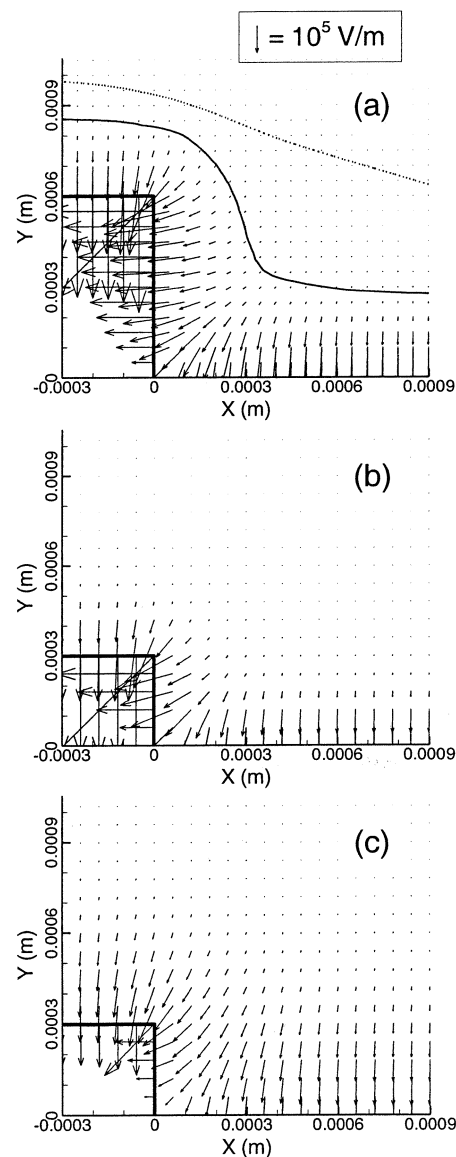


Fig. 5. Electric field vector plots for the conditions of Fig. 4. Note that the electric field inside the solid wall is zero (equipotential surface). The sheath edge is also shown in (a). The solid line corresponds to the location where the relative net charge is 0.01. The dotted line corresponds to the location where the ion speed equals the Bohm speed.

diverge strongly near the step. This divergence has direct implications for ion trajectories near the step, and the resulting IAD function (see below). Importantly, ions spend much of their sheath transit time in regions of strongly divergent fields. Thus, such ions acquire a significant horizontal velocity component, and impact the horizontal plane to the right of the step at large angles with respect to the normal. When the sheath is thin (case a), the electric field is pointing almost horizontally along most of the step sidewall. The highest electric field strength is at the upper right hand corner of the step. One should note a significant difference between the cases of Fig. 5 and the cases that would result for a very small feature height ( $L_{sh}/H \gg 1$ ). For example, in etching of microelectronic devices, feature sizes are below half a micron. In such cases, and for typical sheath thickness of hundreds of micrometers, ions would accelerate under the influence of a vertical (collimated) field for most of their

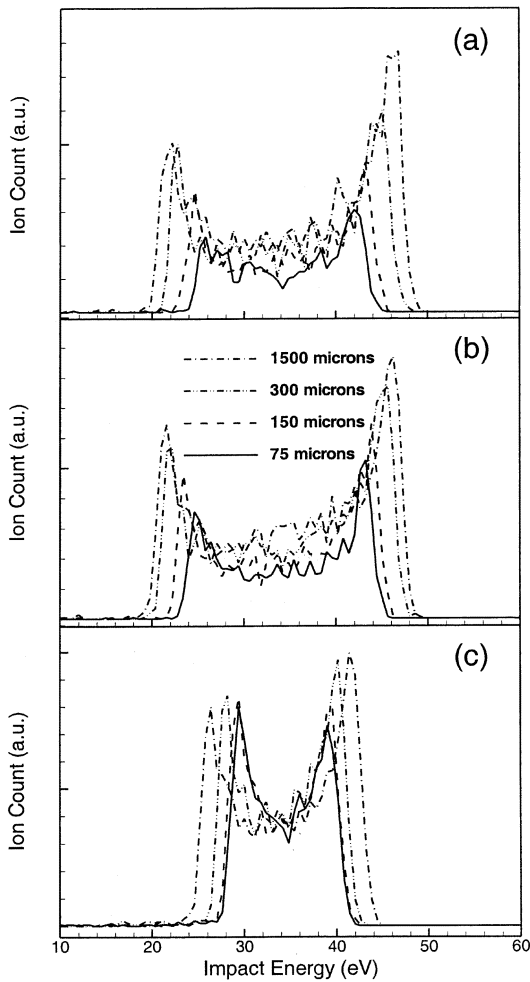


Fig. 6. IEDs obtained by MC simulation at four locations to the right of the step. Cases (a)–(c) correspond to (a)–(c) of Table II.

transit through the sheath. Ions would “feel” the existence of horizontal fields only for the last few microns of their journey. Thus, the expected ion divergence is much weaker in this case [33], [34], [41].

The energy distributions of ions impinging at four locations (75, 150, 300, and 1500  $\mu\text{m}$ ) on the horizontal surface measured to the right of the foot of the step are depicted in Fig. 6. These IEDs were calculated using the MC simulation with the electric field profiles of Fig. 5 as input. Cases (a)–(c) of Fig. 6 again correspond to (a)–(c) of Table II. Characteristic double peaked IEDs are obtained indicative of short (compared to the RF field period) ion transit times through the sheath. Generally, the shape of the IEDs depends on the value of the product  $\omega_{\text{RF}}\tau_{\text{ion}}$ , where  $\omega_{\text{RF}}$  is the applied RF field frequency and  $\tau_{\text{ion}}$  is the ion transit time through the sheath. When  $\omega_{\text{RF}}\tau_{\text{ion}} \ll 1$ , ions cross the sheath in a small fraction of the RF period and sample the instantaneous potential drop across the sheath. The IEDs are double peaked (for a single ion species). When  $\omega_{\text{RF}}\tau_{\text{ion}} \gg 1$ , the ion transit time is very long compared to the field period, and ions sample the time-average sheath potential. The IEDs have a single peak. The IEDs narrow as the plasma density decreases and the sheath thickens, corresponding to a longer ion transit time [compare cases (b) and (c)]. Similarly, for any particular case, the IEDs narrow as one approaches the step starting

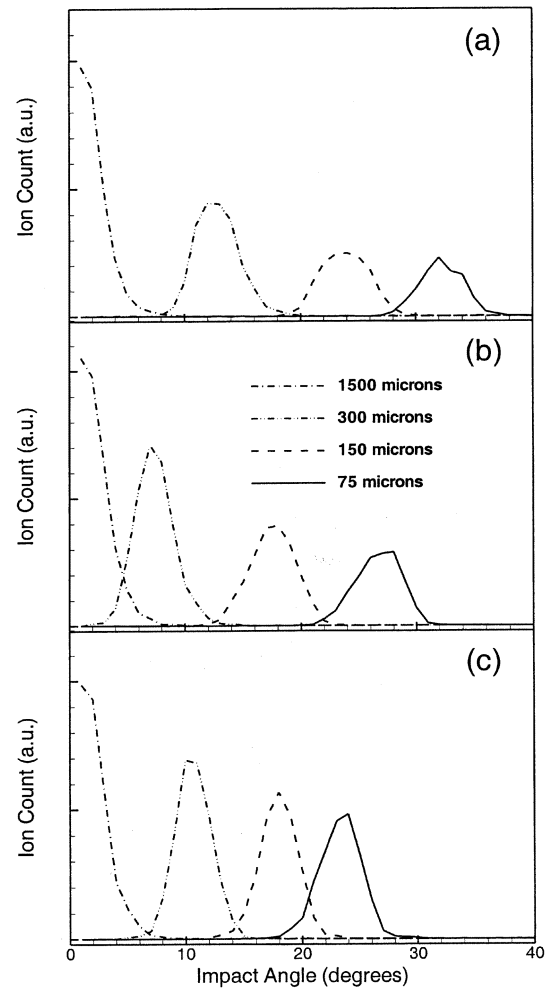


Fig. 7. IADs obtained by MC simulation at four locations to the right of the step. Cases (a)–(c) correspond to (a)–(c) of Table II.

1500  $\mu\text{m}$  away and going 75  $\mu\text{m}$  near the foot of the step. This is due to the fact that the sheath gets thicker as one approaches the step (see also Fig. 4). The ion flux on the horizontal surface (integral of the IEDs) decreases as the step is approached, because ions are diverted away from the vertical and strike the sidewall of the step. It should be mentioned that only the relative values of the IEDs (and IADs) are of interest here; that is why the distributions are not normalized.

The corresponding IADs, calculated by the MC simulation, are shown in Fig. 7. Away from the step (1500  $\mu\text{m}$ ), the IADs are nearly Gaussian centered at zero, reflecting the angular spread of ions emerging from the plasma (several degrees off normal). These ions only see a vertical field. As the step is approached, however, ions see an electric field with a progressively stronger horizontal component, resulting in more ion divergence and a larger impact angle. Fig. 7 also indicates that the ion flux (integral of the IADs) is reduced as the step is approached. Finally, as the  $L_{\text{sh}}/H$  ratio increases [from case (b) to case (c)], ion divergence becomes weaker (smaller impact angles) and the reduction in ion current as the step is approached is not as pronounced.

Fig. 8 depicts the time-average ion flux and ion impact angle (with respect to the vertical) along the surface contour for case

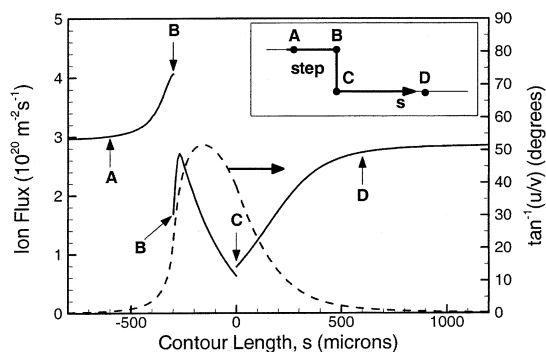


Fig. 8. Time-average ion flux and ion impact angle as a function of contour length along the surface of the substrate, for case (b) of Table II. The ion flux is defined as  $n_i v$  for horizontal surfaces (AB and CD) and  $n_i u$  for sidewall (BC), where  $n_i$  is the ion density and  $u$  and  $v$  are the horizontal and vertical, respectively, ion fluid velocity components. The impact angle is defined as  $\tan^{-1}(u/v)$ .

(b) of Table II calculated by the fluid simulation. The contour length is measured along the surface of the substrate with position zero defined at the foot of the step (point C). Since only the normal component of the ion flux is shown, the flux profile is discontinuous at the two corners (points B and C). As one approaches the step from the left (point A), the ion flux increases from its undisturbed value to its maximum at the upper right corner of the step (point B). Along the sidewall BC, the ion flux increases abruptly to a local maximum near (but not at) the upper right corner, due to the inertia of oncoming ions. The ion flux then drops to its lowest value at the foot of the step (point C) only to increase thereafter to its undisturbed value away from the step (point D). The impact angle is defined as  $\tan^{-1}(u/v)$ , where  $u$  and  $v$  are the horizontal and vertical ion fluid velocities, respectively. The impact angle is zero (i.e., ions arrive along the vertical) away from the step on either side from the sidewall BC, and peaks near the middle of the sidewall. Ions can be deflected by more than  $50^\circ$  off the vertical due to the horizontal component of the electric field (Fig. 5).

In order to quantify the dependence of ion deflection on the system length scales (sheath thickness  $L_{sh}$  and step height  $H$ ), we define  $\theta_{foot}$  as the impact angle of ions at the foot of the step (point C). Fig. 9 shows that  $\theta_{foot}$  decreases linearly as  $L_{sh}/H$  increases up to approximately 3. Then,  $\theta_{foot}$  keeps decreasing (albeit at a smaller rate) as  $L_{sh}/H$  keeps increasing. For very small  $L_{sh}/H$ , the sheath is almost exactly conformal to the step and  $\theta_{foot}$  is  $45^\circ$ . For very large  $L_{sh}/H$ , the surface feature is insignificant, and  $\theta_{foot}$  should approach zero, i.e., ions are barely deflected. Note that the fluid results of Fig. 9 do not account for the distribution of ion angles, which are present even in the absence of a step (due to collisions in the presheath, for example). These were accounted for in the MC simulations of Fig. 7, resulting in a spread of several degrees off normal for ions away from the step where the sheath is planar.

Based on the discussion so far, one might expect that a significant fraction of the oncoming ion flux will strike the sidewall of the step (BC in Fig. 8). These ions will be reflected as neutrals, which will subsequently strike the horizontal surface to the right of the step (CD in Fig. 8). In addition, a fraction of the ion energy will be deposited on the wall, depending on the ion impact angle and the masses of the ion and the wall material [(14)]. Fig. 10

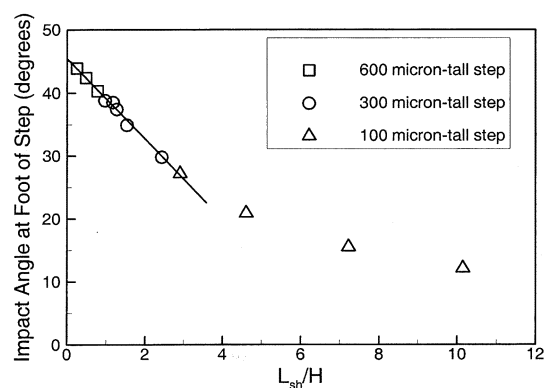


Fig. 9.  $\theta_{foot}$  vs.  $L_{sh}/H$  for all cases listed in Table II. Linear fit to data for  $L_{sh}/H < 3$  is also shown.  $\theta_{foot}$  is the ion impact angle at the foot of the step (point C in Fig. 8).

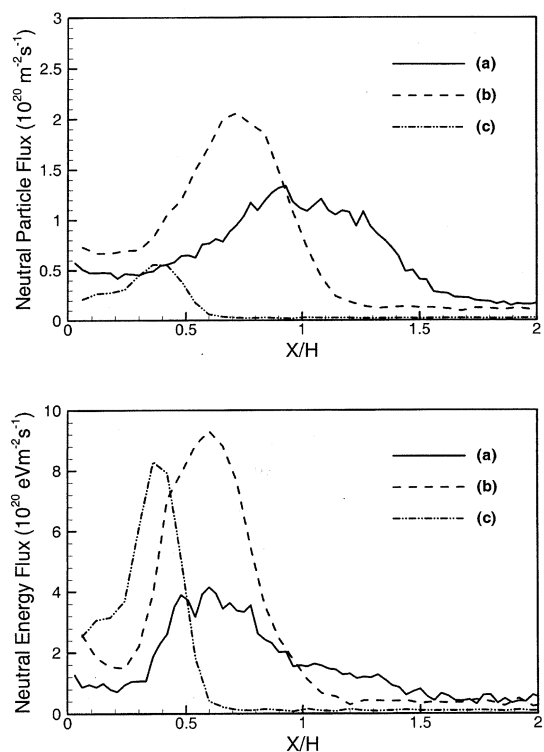


Fig. 10. Particle (top) and energy (bottom) flux of fast neutrals on the horizontal surface to the right of the step sidewall versus normalized distance from the step sidewall. Cases (a)–(c) correspond to (a)–(c) of Table II. The MC simulation yields the relative values of the flux. The absolute values shown here were calculated based on the ion flux found by the fluid simulation.

shows the particle (top) and energy (bottom) flux of fast neutrals on the horizontal surface to the right of the step, as calculated by the MC simulation. Cases (a) to (c) of Fig. 10, correspond to cases (a) to (c), respectively, of Table II. Note that, in the present context, “neutrals” refers to energetic particles resulting by ion neutralization on the sidewalls (and to a much lesser extent, by CX collisions in the gas phase). Thermalized (slow) neutrals are not considered. Far from the step, almost all flux should be due to ions. The energetic neutral flux can be greater than zero, even far away from the step, due to CX collisions depending on gas pressure, ion flux, and sheath thickness). The neutral flux can be comparable to or even larger than the ion flux near the foot of the step (compare to ion fluxes of Fig. 8). As  $L_{sh}/H$  increases

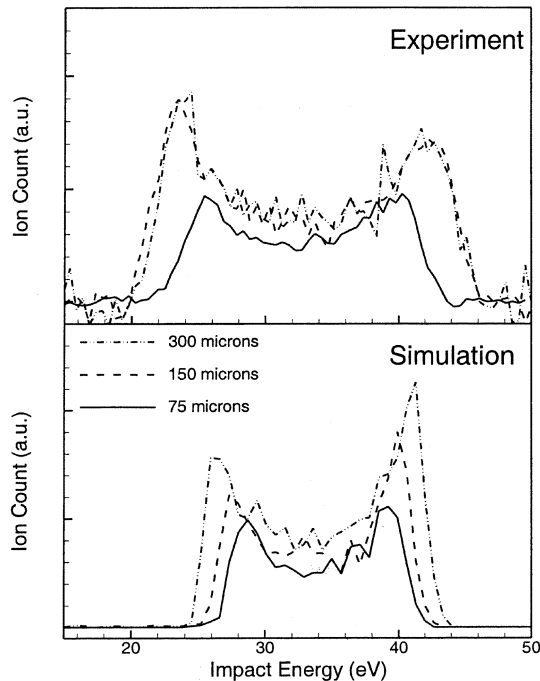


Fig. 11. Comparison between experimental data and simulation predictions of IEDs at three different locations on the horizontal surface to the right of the step sidewall. See text for experimental conditions and simulation parameters.

[going from (a) to (c)], the sheath is less conformal along the step, and ions strike the step sidewall at more grazing angles. Thus, the maximum in the energetic neutral flux occurs closer to the foot of the step and the neutral flux profile does not extend far from the step. Fig. 10 (bottom) shows that the energetic neutrals can retain a significant fraction of the dc sheath potential, resulting in an energy flux of neutrals comparable to that of ions near the step sidewall. This suggests that the reflected neutrals can have considerable effect on the etching or deposition near the step.

#### A. Comparison With Experimental Data

In Figs. 11–13, simulation results are compared with experimental data taken by Woodworth *et al.* [35]. Experiments were carried out in pure Ar discharges in an inductively coupled plasma sustained in a gaseous electronics conference (GEC) reference cell. Using a gridded ion analyzer with a hexagonally packed electrode array detector, the flux, energy, and angular distributions of ions were measured to the right of a 300- $\mu\text{m}$ -tall step. Since the detector elements were shaped in three concentric rings ( $6.4^\circ$ ,  $12.9^\circ$ , and  $19^\circ$  off normal), the angular resolution of the experimental data is rather crude. A double Langmuir probe was used to measure the plasma density and electron temperature in the vicinity of the RF biased chuck. With 5-mtorr gas pressure and 250-W inductive coil power, the plasma density was  $1.3 \times 10^{17} \text{ m}^{-3}$ , the electron temperature was 3.7 eV, and the peak-to-peak voltage between the plasma and chuck was  $21 V_{pp}$ . The parameters used for the simulation were  $n_o = 1.3 \times 10^{17} \text{ m}^{-3}$ ,  $T_e = 3.7 \text{ eV}$ ,  $\Phi_o = 17 + 8 \sin \omega_{RF} t \text{ V}$ ,  $\Phi_w = -16 + 19 \sin \omega_{RF} t \text{ V}$ , and  $f_{RF} = 13.56 \text{ MHz}$ , corresponding to the experimental

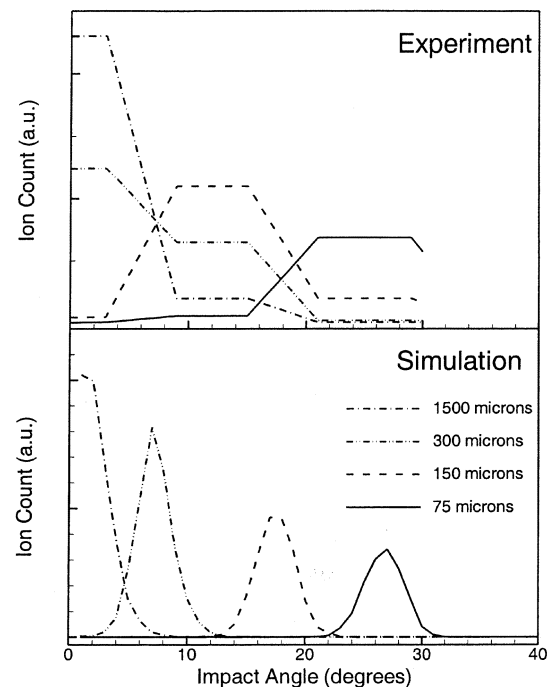


Fig. 12. Comparison between experimental data and simulation predictions of IADs at four different locations on the horizontal surface to the right of the step sidewall. The experimental angular resolution was crude. See text for experimental conditions and simulation parameters.

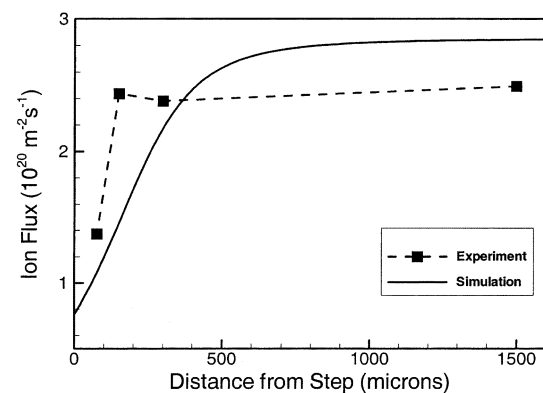


Fig. 13. Comparison between experimental data and simulation predictions of ion flux versus distance on the horizontal surface to the right of the step sidewall. See text for experimental conditions and simulation parameters.

conditions. Reasonable agreement between the experimental data and the model predictions is achieved. All qualitative trends are captured: as one approaches the step from the right, the double peaked IEDs narrow (Fig. 11), the IADs show progressively stronger deflection (larger angles off the normal) of ion trajectories (Fig. 12), and the ion flux decreases (Fig. 13). The simulation is in semiquantitative agreement with the experiment. The discrepancies in the spread of the IEDs (Fig. 11) are probably due to underestimation of the plasma density by the Langmuir probe experiment [35]. When the plasma density in the simulation was doubled, the predicted spread in the IEDs increased to approach the measured one. Errors in plasma density estimations by Langmuir probe measurements are discussed in [36].

## IV. CONCLUSION

A 2-D fluid/MC simulation was developed to study plasma molding over surface topography. The self-consistent fluid simulation included the ion mass and momentum continuity equations coupled to the Poisson equation for the electric potential. The Boltzmann relation was assumed for electrons (no electron inertia). The simulation predicted the evolution of the RF plasma sheath over the surface topography, and the spatiotemporal profiles of the electric field in the region. Using the electric field profiles from the fluid simulation, ions, and energetic neutrals (resulting by ion neutralization on the wall or by CX collisions in the gas phase) were followed by the MC simulation. Using these simulation procedures, ion flow, IEDs, and IADs over an otherwise planar surface with a step were predicted. The step height was comparable to the sheath thickness for the high-density RF argon plasma considered. As one approached the vertical wall of the step, the ion flux decreased, the double-peaked IEDs narrowed, and the IADs indicated strong deflection of ions toward the (vertical) sidewall of the step. This was due to strong horizontal components of the electric field near the step, coupled with the fact that ions spend a sizable fraction of their sheath transit time under the influence of these fields. The ion impact angle at the foot of the step scaled with the ratio of sheath thickness to step height. The energetic neutral flux was found to be comparable to the ion flux on the horizontal surface to the right of the step sidewall. Simulation results were in good agreement with experimental data on ion flux, IEDs, and IADs near the step.

## REFERENCES

- [1] S. M. Rosnagel, J. J. Cuomo, and W. D. Westwood, Eds., *Handbook of Plasma Processing Technology*. Park Ridge, NJ: Noyes, 1990.
- [2] M. A. Lieberman and A. J. Lichtenberg, *Principles of Plasma Discharges and Materials Processing*. New York: Wiley, 1994.
- [3] D. J. Economou, "Modeling and simulation of plasma etching reactors for microelectronics," *Thin Solid Films*, vol. 365, pp. 348–367, 2000.
- [4] P. A. Miller and M. E. Riley, "Dynamics of collisionless rf plasma sheaths," *J. Appl. Phys.*, vol. 82, pp. 3689–3709, 1997.
- [5] E. Kawamura, V. Vahedi, M. A. Lieberman, and C. K. Birdsall, "Ion energy distributions in rf sheaths; review, analysis and simulation," *Plasma Sources Sci. Technol.*, vol. 8, pp. R45–R64, 1999.
- [6] M. J. Kushner, "Distribution of ion energies incident on electrodes in capacitively coupled rf discharges," *J. Appl. Phys.*, vol. 58, pp. 4024–4031, 1985.
- [7] B. E. Thomson, H. H. Sawin, and D. A. Fisher, "Monte Carlo simulation of ion transport through rf glow-discharge sheaths," *J. Appl. Phys.*, vol. 63, pp. 2241–2251, 1988.
- [8] M. S. Barnes, J. C. Forster, and J. H. Keller, "Ion kinetics in low-pressure, electropositive, rf glow discharge sheaths," *IEEE Trans. Plasma Sci.*, vol. 19, pp. 240–244, Jan. 1991.
- [9] J. Hopwood, "Ion bombardment energy distributions in a radio frequency induction plasma," *Appl. Phys. Lett.*, vol. 62, pp. 940–942, 1993.
- [10] M. A. Sobolewski, J. K. Olthoff, and Y. Wang, "Ion energy distributions and sheath voltages in a radio-frequency-biased, inductively coupled, high-density plasma reactor," *J. Appl. Phys.*, vol. 85, pp. 3966–3975, 1999.
- [11] E. K. Edelberg, A. Perry, N. Benjamin, and E. S. Aydil, "Energy distribution of ions bombarding biased electrodes in high density plasma reactors," *J. Vac. Sci. Technol. A*, vol. 17, pp. 506–516, 1999.
- [12] J. R. Woodworth, M. E. Riley, P. A. Miller, G. A. Hebner, and T. W. Hamilton, "Ion energy and angular distributions in inductively driven discharges in chlorine," *J. Appl. Phys.*, vol. 81, pp. 5950–5959, 1997.
- [13] I. W. Rangelow and H. Loschner, "Reactive ion etching for microelectrical mechanical system fabrication," *J. Vac. Sci. Technol. B*, vol. 13, pp. 2394–2399, 1995.
- [14] U. Czarnetzki, G. A. Hebner, D. Luggenholtscher, H. F. Dobebe, and M. E. Riley, "Plasma sheath electric field strengths above a grooved electrodes in a parallel plate radio-frequency discharge," *IEEE Trans. Plasma Sci.*, vol. 27, pp. 70–71, Feb. 1999.
- [15] D. Kim and D. J. Economou, "Plasma molding over surface topography," *JSME Int. J., B*, vol. 45, pp. 117–122, 2002.
- [16] S. Panda, D. J. Economou, and L. Chen, "Anisotropic etching of polymer films by high energy ( $\sim 100$ s of eV) oxygen atom neutral beams," *J. Vac. Sci. Technol. A*, vol. 19, pp. 398–404, 2001.
- [17] F. F. Chen, *Introduction to Plasma Physics and Controlled Fusion Volume 1: Plasma Physics*. New York: Plenum, 1984.
- [18] M. Hong and G. A. Emmert, "Two-dimensional fluid modeling of time-dependent plasma sheath," *J. Vac. Sci. Technol. B*, vol. 12, pp. 889–896, 1994.
- [19] P. Vitello, C. Cerjan, and D. Braun, "Flow: A two-dimensional time-dependent hydrodynamical ion extraction model," *Phys. Fluids B*, vol. 4, pp. 1447–1456, 1992.
- [20] P. J. Roache, *Fundamentals of Computational Fluid Dynamics*. Albuquerque, NM: Hermosa, 1998.
- [21] J. P. Boris and D. L. Book, "Flux-corrected transport. I. SHASTA, A fluid transport algorithm that works," *J. Comput. Phys.*, vol. 11, pp. 38–69, 1973.
- [22] S. T. Zalesak, "Fully multidimensional flux-corrected transport algorithm for fluids," *J. Comput. Phys.*, vol. 31, pp. 335–362, 1979.
- [23] S. K. Dhali and P. F. Williams, "Two-dimensional studies of streamers in gases," *J. Appl. Phys.*, vol. 62, pp. 4696–4707, 1987.
- [24] J. V. DiCarlo and M. J. Kushner, "Solving the spatially dependent Boltzmann's equation for the electron-velocity distribution using flux corrected transport," *J. Appl. Phys.*, vol. 66, pp. 5763–5774, 1989.
- [25] W. H. Press, S. A. Teukolsky, W. T. Vetterling, and B. P. Flannery, *Numerical Recipes in Fortran*. Cambridge, U.K.: Cambridge, 1992.
- [26] K.-U. Riemann, "Kinetic theory of the plasma sheath transition in a weakly ionized plasma," *Phys. Fluids*, vol. 24, pp. 2163–2172, 1982.
- [27] C. K. Birdsall, "Particle-in-cell charged-particle simulations, plus Monte Carlo collisions with neutral atoms, PIC-MCC," *IEEE Trans. Plasma Sci.*, vol. 19, pp. 65–85, Feb. 1991.
- [28] H. Niehus, W. Heiland, and E. Taglauer, "Low-energy ion scattering at surfaces," *Surf. Sci. Report*, vol. 17, pp. 213–303, 1993.
- [29] S. R. Kasi, M. A. Kilburn, H. Kang, J. W. Rabalais, L. Tavernini, and P. Hochmann, "Interaction of low energy reactive ions with surfaces. III. Scattering of 30–200 eV Ne<sup>+</sup>, O<sup>+</sup>, C<sup>+</sup>, and CO<sup>+</sup> from Ni(111)," *J. Chem. Phys.*, vol. 88, pp. 5902–5913, 1988.
- [30] G. S. Hwang, C. M. Anderson, M. J. Gordon, T. A. Moore, T. K. Minton, and K. P. Giapis, "Gas-surface dynamics and profile evolution during etching of silicon," *Phys. Rev. Lett.*, vol. 77, pp. 3049–3052, 1996.
- [31] B. A. Helmer and D. B. Graves, "Molecular dynamics simulations of Ar<sup>+</sup> and Cl<sup>+</sup> impacts onto silicon surfaces: Distributions of reflected energies and angles," *J. Vac. Sci. Technol.*, vol. 16, pp. 3502–3514, 1998.
- [32] W. Choi, C. Kim, and H. Kang, "Interactions of low energy (10–600 eV) noble gas ions with a graphite surface: Surface penetration, trapping and self-sputtering behaviors," *Surf. Sci.*, vol. 281, pp. 323–335, 1993.
- [33] D. J. Economou and R. C. Alkire, "Effect of potential field on ion deflection and shape evolution of trenches during plasma-assisted etching," *J. Electrochem. Soc.*, vol. 135, pp. 941–949, 1988.
- [34] S. G. Ingram, "The influence of substrate topography on ion bombardment in plasma etching," *J. Appl. Phys.*, vol. 68, pp. 500–504, 1990.
- [35] J. R. Woodworth, P. A. Miller, R. J. Shul, I. C. Abraham, B. P. Aragon, T. W. Hamilton, C. G. Willison, D. Kim, and D. J. Economou, "An experimental and theoretical study of ion distributions near 300- $\mu$ m-tall-steps on rf-biased wafers in high density plasmas," *J. Vac. Sci. Technol.*, to be published.
- [36] P. A. Miller, G. A. Hebner, K. E. Greenberg, P. D. Pochan, and B. P. Aragon, "An inductively coupled plasma source for the gaseous electronics conference RF reference cell," *J. Res. Natl. Inst. Stand. Technol.*, vol. 100, pp. 427–439, 1995.
- [37] T. Panagopoulos and D. J. Economou, "Plasma sheath model and ion energy distribution for all radio frequencies," *J. Appl. Phys.*, vol. 85, pp. 3435–3443, 1999.
- [38] A. Metze, D. W. Ernie, and H. J. Oskam, "The energy distribution of ions bombarding electrode surfaces in rf plasma reactors," *J. Appl. Phys.*, vol. 65, pp. 993–998, 1989.
- [39] J. Liu, G. L. Huppert, and H. H. Sawin, "Ion bombardment in rf plasmas," *J. Appl. Phys.*, vol. 68, pp. 3916–3934, 1990.
- [40] D. T. K. Kwok, Z. M. Zenh, P. Chu, and T. E. Sheridan, "Effects of tube length and radius for inner surface plasma immersion ion implantation using an auxiliary electrode," *IEEE Trans. Plasma Sci.*, vol. 27, pp. 225–238, Jan. 1999.

- [41] M. Ardehali and H. Matsumoto, "Influence of surface topography on ion trajectories in low-pressure plasma etching," *J. Appl. Phys.*, vol. 72, pp. 4995–4997, 1992.

**Doosik Kim** was born in Seoul, Korea, in 1970. He received the B.S. and M.S. degrees in chemical engineering from Seoul National University, Korea, in 1992 and 1996, respectively. He is currently pursuing the Ph.D. degree at the University of Houston, Houston, TX.

His research interests include modeling and multidimensional simulation of plasma molding over complex surface topography, Monte Carlo simulations, ion energy and angular distributions in radio frequency plasma sheaths, and glow discharge plasma reactor simulations.

**Demetre J. Economou** received the M.S. and Ph.D. degrees in chemical engineering from the University of Illinois at Urbana-Champaign, IL, in 1983 and 1986, respectively.

Since 1986, he has been with the Chemical Engineering Department at the University of Houston. His research interests include plasma reactor modeling and simulation, plasma diagnostics, ion–ion plasmas, neutral beam processing, atomic layer etching, plasma-surface interactions, and chemical vapor deposition. He is the author or coauthor of over 120 papers and book chapters in these areas.